AIAA JOURNAL
Vol. 45, No. 7, July 2007

Multidisciplinary Design Optimization for Hypersonic Experimental Vehicle

Takeshi Tsuchiya* and Yoichi Takenaka†
University of Tokyo, Tokyo 113-8656, Japan
and
Hideyuki Taguchi‡
Japan Aerospace Exploration Agency, Tokyo 182-8522, Japan

DOI: 10.2514/1.26668

The purpose of this study is to apply a multidisciplinary optimization method for the conceptual designs of hypersonic experimental vehicles with advanced airbreathing engines. Using this method, we obtain the necessary vehicle sizes and optimal flight trajectories. The vehicle has a lifting body shape. First, we integrate analytical methods into the optimization problem, the solution of which yields the smallest gross weight of the vehicle. The results indicate a vehicle that is about 12 m in total length and 4–5 Mg in gross weight. This information allows us to determine the optimal vehicle configuration and flight trajectory for a highly feasible hypersonic vehicle. In addition, the trajectory optimizations enable the vehicle to glide back to a takeoff point without consuming propellant. This study confirms the effectiveness of the proposed analysis and optimization method.

Nomenclature

A_{PCTJ}	=	engine intake area
C_D	=	drag coefficient
$\boldsymbol{C}_E$	=	equality constraint function
$\boldsymbol{C}_I$	=	inequality constraint function
C_L	=	lift coefficient
C_M	=	pitching moment coefficient
$C_{p\mathrm{base}}$	=	base pressure
c_w	=	wing root chord length
D	=	drag
f	=	approximate function in response surface model
h_f	=	fuselage height
I_{SP}	=	specific impulse
L	=	lift
l_f	=	fuselage length
M	=	pitching moment
M_∞	=	Mach number of main flow
N_p	=	number of input variables in response surface model
N_s	=	number of sample points in response surface model
$\boldsymbol{p}$	=	input variable in response surface model
q	=	dynamic pressure
S	=	wing area
$\mathbf{s}_i$	=	sample point in response surface model ($i = 1, 2, \ldots, N_s$)
w_f	=	fuselage width
w_i	=	weight parameter in response surface model ($i = 1, 2, \ldots, N_s$)
$\boldsymbol{x}$	=	design variables
α	=	angle of attack
β_j	=	radius of the Gaussian in response surface model ($j = 1, 2, \ldots, N_p$)
δ_e	=	elevon deflection
θ_f	=	angle between undersurface ramp and the body axis
Λ	=	wing sweepback angle

Received 20 July 2006; revision received 30 March 2007; accepted for publication 1 April 2007.

*Associate Professor, Department of Aeronautics and Astronautics; tsuchiya@mail.ecc.u-tokyo.ac.jp. Member AIAA.
†Graduate Student, Department of Aeronautics and Astronautics.
‡Senior Researcher, Supersonic Transport Team, Aviation Program Group; taguchi.hideyuki@jaxa.jp. Member AIAA.

I. Introduction

THE aircraft design process integrates various special analyses, including those of aerodynamics, structure, propulsion, trajectory, controls, cost, and operations. Because advanced aircraft of the future are designed at the limits of present technologies, the latest computational analysis technologies in each discipline must be used efficiently and optimization techniques must be applied. The application of optimization methods to multidisciplinary analysis is referred to as multidisciplinary design optimization (MDO). With advances in computers, various MDO methods have been applied widely, from the design of components to that of aircraft overall [1]. This paper implements MDO for the design of hypersonic vehicles.

In April 2005 the Japan Aerospace Exploration Agency (JAXA) presented its long-term vision over the next 20 years. The vision includes demonstrations of hypersonic aircraft that can cross the Pacific Ocean in two hours at Mach 5. Engines that can propel the aircraft at such speeds are now being researched and developed. A candidate for such engines is the precooled turbojet (PCTJ) engine; it can reach about Mach 6 [2]. The PCTJ engine has a precooling heat exchanger in front of a turbojet engine to reduce the air temperature by the cooling capacity of liquid hydrogen (propellant of the engine). The air temperature at Mach 6 through the heat exchanger is almost equivalent to that at Mach 3. The precooling also increases the air density, thereby significantly boosting the engine's thrust. To enhance the precooling effect, fuel rich operation is required. This also increases the thrust, despite a small loss of the specific impulse. We have studied the components of the PCTJ engine, and our next step is to examine it in an actual flight environment [3].

One of our plans is a flight test of a hypersonic experimental vehicle that has the capability of horizontal takeoff and landing by the PCTJ engine. The goal is a performance test of the engine in acceleration and ascent up to Mach 5. The purpose of this paper is to consider the optimal vehicle scale and trajectory that satisfies the required constraint conditions and has the highest feasibility. This study solves a multidisciplinary design optimization problem in which we simultaneously optimize both the configurations and trajectories of the vehicles. One of features of the analytical technique in this study is that it uses an approximation model of the aerodynamics analysis to speed up optimization. First we explain the analytical tools: the vehicle definition, the weight estimation, and the analyses of aerodynamics, propulsion, and trajectory. Next we define

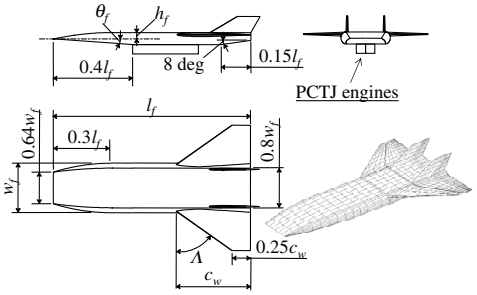

Fig. 1 Vehicle layout.

a design optimization problem to obtain highly feasible vehicles. Finally we consider the optimal solutions and their significance.

II. Analytical Method and Optimization Problem

The hypersonic experimental vehicle in this study (Fig. 1) has a shape similar to that of NASA's X-43A. This figure also indicates the geometric parameters that we have to specify. The other design variables are flight performance parameters and flight trajectory variables, which are given in Table 1. In this study we optimize acceleration and return trajectories; the design variables contain state and control variables of the flight trajectories.

Figure 2 shows the analytical process. Each analysis calculates output values for the subsequent analysis from the values of the design variables and the input values obtained from the previous analysis. In addition, it computes the function values of equality and inequality constraint conditions ($\boldsymbol{C}_E$ and $\boldsymbol{C}_I$ in Fig. 2), which the design variables of the completed vehicle must satisfy. Though the values we find for the design variables must satisfy all the constraint conditions, we cannot always obtain unique values. Therefore we give a figure of merit and define an optimization problem to find the best values under the criterion. The gross weight of the vehicle is defined as a minimized performance index. As the gross weight has a strong relationship to the development cost, we investigate the feasibility of the hypersonic vehicles on the basis of the gross weight.

A sequential quadratic programming method is employed as an optimization method. There are more than 8000 optimized design variables. The reason for the large number is that there are not only the geometric and flight performance parameters, but also the discretized state and control variables. The following paragraphs summarize the analytical methods and constraint conditions.

A. Vehicle Definition

The hypersonic experimental vehicle is shaped like the X-43A. The PCTJ engines are suspended on the undersurface parallel to the body axis. To deliver air uniformly to the intakes, the undersurface of the fuselage is flat. The number of engines is essentially one of the design variables; however the optimization method in this paper can optimize only continuous variables and not a discrete number of integer variables. Thus we determine the number beforehand. The number and the performance of the PCTJ engine are detailed in the propulsion analysis. The profile of the main wing and the vertical tails is NACA0005. We suppose that an elevon makes up 25% of the wing tip chord and 90% of the exposed wing semispan. As shown later, the elevon has size enough to attain pitch trim during the flight. We also suppose that the area of the vertical tail fins is 13% that of the main wing.

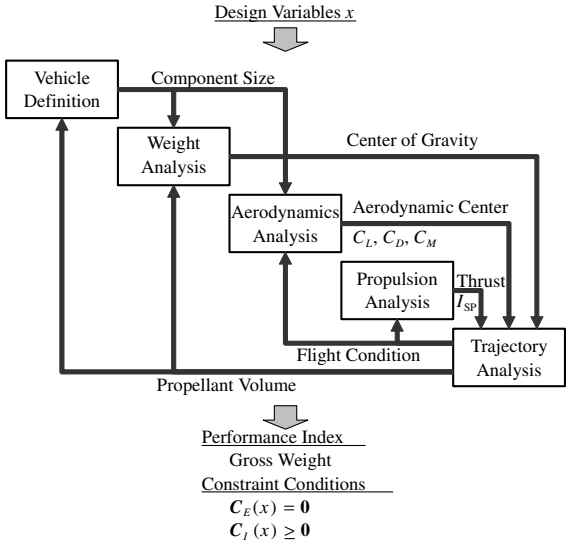

Fig. 2 Analytical process.

The vehicle definition calculates detailed component sizes of the vehicle from the geometric parameters included in the design variables for the weight analysis and the aerodynamics analysis. In addition, to attain the proper vehicle shape, the vehicle definition computes inequality constraints for the geometric parameters. At the same time, the trajectory analysis gives the amount of propellant (liquid hydrogen) and the vehicle definition calculates the required tank size accordingly. A constraint condition demands that the fuselage should be large enough to hold the tank. According to traditional design examples of hypersonic aircraft [4], we suppose that the proportion of the tank volume to the fuselage volume is less than 50%. As a result, however, the proportion of optimal vehicles is the upper limit, 50%.

B. Weight Analysis

The weight analysis computes the vehicle's component weights based on the geometric and flight performance parameters in the design variables, the component sizes given by the vehicle definition and the amount of propellant. In addition, component allocation in the vehicle makes it possible to compute the center of gravity (c.g.) location as the propellant weight changes. The trajectory analysis uses the c.g. location to check longitudinal static stability. In this study we employ the hypersonic aerospace sizing analysis (HASA) program [4], a statistical weight estimation method, with the following modifications.

HASA classifies vehicles' subsystems into four components: actuator, avionics, electrical system, and equipment. Because the subsystem weights estimated for small-scale vehicles such as the one in this study are clearly too large, the weights are not estimated with good accuracy. HASA also indicates that the subsystems of most vehicles weigh 5–10% of gross weight. Thus this study estimates the subsystem weight at 10% of gross weight. Because the subsystems

Table 1 Design variables of vehicle configuration and flight trajectory

Parameter type	Variable
Geometry (cf. Fig. 1)	l_f, w_f, h_f, θ_f, c_w, Λ
	Engine's intake area A_{POTJ}
Flight performance	Gross weight
	Maximum thrust
	Maximum normal load factor
Flight trajectory	Discretized state variables
	Discretized control variables
	Terminal times of acceleration phase and return phase

are put all over the vehicle, those c.g. are assumed to be corresponding to the c.g. of the vehicle. Furthermore the weight of the PCTJ engine, which is not included in HASA, is estimated by a simplified design calculation. The weight of the engine, which is a heavy component, has a great influence on the c.g. of the vehicle. To put the c.g. forward for static stability, the engines are located at the front of the undersurface.

Estimation of the component weights requires the gross weight, which is the sum total of the component weights. For example, the landing gear weight, as a part of the gross weight, is expressed as an equation with the gross weight. Thus we include the gross weight in the design variables, with which the method analyzes the component weights. We define an equality constraint condition such that the sum of the component weights corresponds exactly to the gross weight in the design variables.

C. Aerodynamics Analysis

The aerodynamics analysis computes the lift, drag, pitching moment, and aerodynamic center, all of which are required for the flight trajectory analysis. These data are calculated from the geometric parameters, component sizes, flight Mach number, angle of attack, and elevon deflection. As the aerodynamics analysis requires surface panels of the airframe, we developed a program that automatically generates them from the geometric parameters and component sizes. For computing subsonic aerodynamic characteristics, we employ a widely used aerodynamic panel code PANAIR [5], that is, a high-order panel method. In supersonic and hypersonic flow, we apply a tangent-cone method [6] and the Prandtl–Meyer expansion theory [7]. The tangent-cone method, which is applicable in impact flow region, assumes that the static pressure on a surface panel is equivalent to the pressure on a cone with a semivertex angle that is equal to the angle between the flow direction and the tangent to the panel. In contrast, the Prandtl–Meyer expansion theory computes the static pressure on a panel in shadow flow region from Prandtl–Meyer expansion. References [8,9] show that the surface static pressures computed in these methods are in good agreement with those measured in experiments, and that all of the longitudinal results can be of some use in conceptual design studies.

We also compute the base drag and the skin friction drag. Because the base pressure of the vehicle is not computable in the above methods, we apply the following empirical formulas [10] based on flight experiments of X-15, the space shuttle, and lifting body vehicles.

$$C_{p\text{base}} = \begin{cases} -0.139 - 0.419(M_\infty - 0.161)^2 & \text{if } M_\infty \le 1 \\ -M_\infty^{-2} + 0.57M_\infty^{-4} & \text{if } M_\infty > 1 \end{cases} \tag{1}$$

The skin friction drag is computed from integrating the friction coefficients of the surface panels that are based on a simple calculation method of a friction coefficient of compressive fluid flowing on a flat plate in [11]. The flow condition on the panel, which is necessary for computing the friction coefficients, is computed with the above methods. Transonic aerodynamic forces are interpolated from subsonic and supersonic forces.

These methods in conceptual designs are less accurate than recent computational fluid dynamics (CFD) methods. For example, the study does not consider the interference drag caused by the coupling of the airframe and engines. Because the engine is contained in a box-shaped casing, the interference drag is probably small, but it is difficult to estimate it accurately. The exact estimation is a future study. In the future, we must verify these methods with higher fidelity CFD methods and wind tunnel tests.

Now we can incorporate these methods into the MDO framework. However though the computational costs of the methods used in this study are lower than those of the CFD methods, they consume much computation time because the iterative optimization process makes numerous aerodynamic analyses. Therefore we introduce a response surface method.

Table 2 Parameter combination of the constructed response surfaces

Parameters	Values
Aerodynamic characteristics	L/q, D/q, M/q
Mach numbers	0.3, 0.7, 0.9, 1.1, 3.0, 4.0, 5.0, 6.0
(α, δ_e) deg	(0, 0), (4, 0), (8, 0), (0, −8)

D. Response Surface Method

To reduce the computation time for the aerodynamics analysis in the iterative optimization process, we construct response surfaces that give aerodynamic coefficients based on the geometric parameters and flight conditions before the optimization process. This subsection summarizes the response surface method in this study.

Table 2 shows the respective Mach numbers, angles of attack α, and elevon deflections δ_e from which the response surfaces are constructed. As we need to analyze three aerodynamic characteristics (L/q, D/q, and M/q), we must construct 96 response surfaces in total. The output of the response surface to obtain the lift is not lift coefficient C_L but L/q. Because the wing area S of the vehicle in this study is smaller than those of usual aircraft, we consider it preferable to construct the response surface $L/q = C_L S$ including S instead of C_L for improving approximate accuracy. Though the input variables of the response surfaces are the geometric parameters in the design variables, the response surface has only five input variables (w_f, h_f, θ_f, c_w, Λ) by fixing the fuselage length l_f to be 10 m because of their scaling relationship. This paper proposes the response surface model with radial basis functions [12]. In this model, we choose a small number of sample points $\boldsymbol{s}_1, \ldots, \boldsymbol{s}_{N_s}$ of the input variables, and then we approximate the relation between the input variables $\boldsymbol{p}(\in \boldsymbol{x})$ and an aerodynamic characteristic $f(\boldsymbol{p})$ by a linear combination of the Gaussian:

$$f(\boldsymbol{p}) = \sum_{i=1}^{N_s} w_i \prod_{j=1}^{N_p} \exp\left[-\frac{(p_j - s_{ij})^2}{\beta_j^2}\right] \tag{2}$$

where N_p (=5) is the number of the input variables $\boldsymbol{p} = [p_1, \ldots, p_{N_p}]^T$, β_j is a radius of the Gaussian, and w_i is a weight parameter.

The arrangement of the sample inputs $\boldsymbol{s}_i$ and the values of β_j and w_i are optimized based on the algorithms proposed in [13]. In this study, the number of sampling points is 15 to 30 for attaining the normalized mean square error, which is the mean square error of the approximation normalized by the variance of the analysis, less than 1×10^{-2}. Figure 3 indicates approximate accuracies of a response surface providing L/q at Mach number 0.3, angle of attack 0 deg, and elevon deflection 0 deg. Each plot in this figure suggests an output of the original analysis and an output $f(\boldsymbol{p})$ of the response surface model for a random input $\boldsymbol{p}$. A good agreement suggests the constructed response surface model has excellent approximate accuracy.

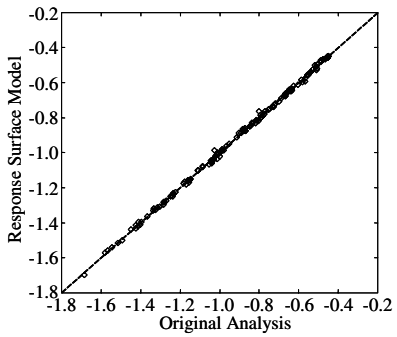

Fig. 3 Comparison of the output values of the response surface model and original analysis L/q at Mach 0.3 and $(\alpha, \delta_e) = (0, 0)$.

The aerodynamic coefficients for a given Mach number, angle of attack, and elevon deflection are calculated from the outputs of the response surfaces for inputs of the geometric parameters as follows. We approximate the equations of the lift and pitching moment coefficients as second-order polynomials of the angle of attack and as first-order polynomials of the elevon deflection. In contrast, the drag is represented as a quadratic function of the angle of attack and elevon deflection. First we compute the coefficients of the polynomials that yield the aerodynamic coefficients in each sampling Mach number. Next the interpolation of the equations obtained in the sampling Mach numbers yields the aerodynamic coefficients in the given Mach number, angle of attack, and elevon deflection.

E. Propulsion Analysis

Given a flight altitude and Mach number from the trajectory analysis, the propulsion analysis calculates the thrust force and specific impulse of the PCTJ engine. JAXA provides tables of the thrust force per intake area and the specific impulse in response to Mach number and altitude [2]. The performance models include ram drag on the intake and pressure loss in the precooler. The intake area, to which the thrust force generated by one engine is proportional, is one of the design variables. This study assumes that the engine can be throttled between zero and maximum rated thrust. Throttling decreases the specific impulse, but for the sake of simplicity we do not consider that effect.

In supersonic cruise of the vehicles in this study, after the air is compressed and expanded at the front and back of the ramp, the air entering the engines on the undersurface of the fuselage has the almost same condition as the main flow, because the angle of attack in optimal flights is small and the engines are attached parallel to the body axis. In addition, because flight speed of the vehicles is lower than X-43A flying at Mach 7 to 10, the effect of forebody compression is smaller than that of X-43A. Therefore we assume that an engine inlet condition is equivalent to a main flow condition. On the other hand, pressure increase on an expansion surface (aftbody) by engine exhaust is not considered in this paper. This effect increases lift and thrust, which means this study underestimates the vehicle performance. Modeling these effects of the fore- and aftbody is a future work. This paper considers two cases: two-engine vehicles and four-engine vehicles.

F. Trajectory Analysis

In this study we implement three-degrees-of-freedom (3DOF) trajectory analysis [14]. The equations of motion consist of seven state variables (altitude, downrange, crossrange, velocity, flight path angle, azimuth angle, and mass) and four control variables (angle of attack, elevon deflection, bank angle, and throttle). The reason why the control variables include the elevon deflection, which is not necessary for 3DOF analysis, is explained later. Although we disregard the effects of the curve of the Earth and its rotation, we take centrifugal force into account. In addition, the analysis includes the U.S. standard atmosphere and the gravity model in which acceleration is inversely proportional to the square of geocentric altitude. As described above, we optimize the flight trajectory with the other design variables. The trajectory analysis must deal with dynamic variables (the state and control variables), which depend on time, whereas the other design variables are static and independent of time. Therefore we employ a direct collocation method [15]. The state and control variables are discretized to transform them into such static variables as the other design variables. In the same manner, we also discretize constraint conditions and the motion equations expressed as differential equations, which are functions of the state and control variables. The number of discrete elements is about 800 in this study.

Vehicles capable of flying along the following profiles are obtained through the trajectory analysis. The vehicle with the PCTJ engines takes off, accelerates to Mach 5, then flies back to the takeoff point while decelerating. It follows that the flight trajectory is divided into two phases: an acceleration phase and a return phase. We define two cases of flight profiles. In case 1, no limitation is given to the bank angle in the acceleration phase. As shown in the next section, the unconstrained bank angle provides a climbing turn in the acceleration phase. In such an optimal trajectory, a rapid change of the bank angle causes slipping flow, which disturbs the uniformity of flow. Therefore we consider it preferable to make a straight flight in the ascent phase because a uniform influx of air into the intakes is necessary to measure engine performance accurately. In case 2, we suppose that the bank angle is fixed to zero in the acceleration phase. We solve four optimization problems, because the vehicle has either two or four engines and there are two cases in the acceleration phases.

The initial conditions of the acceleration phase are related to acceleration on a runway and takeoff from the ground. We suppose that the takeoff speed is not specified, takeoff length is less than 2000 m, and the total of the vehicle's upward forces balances with its weight at takeoff. The terminal condition of the acceleration phase is that the vehicle's flight speed coincides with Mach 5. The initial condition of the return phase is continuity in the state and control variables. The terminal conditions of the return phase include leaving 5% of the total propellant weight as a margin. Moreover the terminal coordinates of the vehicle must coincide with those of the takeoff point. Although the terminal azimuth angle in case 1 is equal to that at takeoff, the difference between the initial and terminal azimuth angles in case 2 is 180 deg. We explain later why the definition of the terminal azimuth angles differs.

The constraint conditions in both the phases are that the angle of attack must be between 0 and 10 deg, the elevon deflection must range between −10 and 10 deg, the dynamic pressure must be less than 50 kPa, and the thrust and the normal load factor must be below the respective maximum values. These maximum values, which are related to the structural weight of the vehicle, are included in the optimized flight parameters. In addition, the vehicle always satisfies the trim condition that the pitting moment is zero with the elevon and the longitudinal static stability condition that the c.g. is in front of the aerodynamic center. We can compute the angle of attack and elevon deflection satisfying the trim condition. The trim condition adds an approximative rigid-body model to the simple point-mass model of the vehicle, which can analyze the flight trajectory more accurately. It is because the elevon deflection besides the angle of attack is one of the control variables. Moreover we impose 0 deg on the bank angle in the acceleration phase of case 2.

III. Optimal Solutions

A. Case 1: Turning Flight in the Acceleration Phase

This subsection shows the optimal solutions of the two- and four-engine vehicles, whose bank angles are unconstrained in the acceleration phase. Table 3 indicates configurations and component weights of the optimal vehicles, as illustrated in Figs. 4 and 5. The vehicles are approximately 12 m in total length and 4–5 Mg in gross

Table 3 Optimal configurations and component weights of case 1

Parameters	Two-engine vehicle	Four-engine vehicle
l_f, m	11.97	12.39
w_f, m	1.80	1.97
h_f, m	0.36	0.37
θ_f, deg	3.0	3.0
c_w, m	2.99	3.10
Λ, deg	53.3	55.7
A_{POTJ}, m^2	0.393	0.528
Fuselage, kg	452	521
Wing, kg	113	154
Vertical tail, kg	47	51
PCTJ, kg	1751	2647
Thrust structure, kg	61	72
Tank, kg	161	186
Thermal protection system, kg	198	215
Landing gear, kg	105	147
Subsystem, kg	374	506
Propellant, kg	482	558
Gross weight, kg	3744	5057

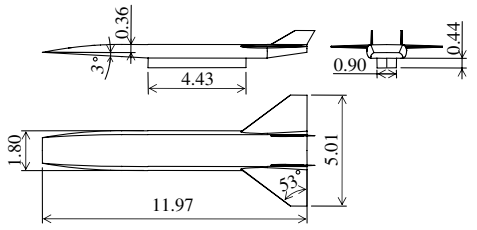

Fig. 4 Optimal two-engine vehicle.

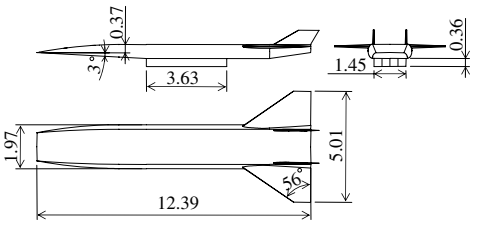

Fig. 5 Optimal four-engine vehicle.

weight. The four-engine vehicle is slightly larger than the two-engine vehicle, but both vehicles are similar, with a long fuselage and small wings. There are three reasons why such long and slender bodies are optimal.

The first reason is low structural weight. Although a short and fat fuselage, which can bear a large bending moment, probably decreases fuselage weight, it increases wing weight because it involves a large wing carry through. From the relationship between fuselage weight and wing weight, the weight analysis in this study reveals that the vehicle with a long and slender fuselage is lighter. The second reason is its low drag and high lift-to-drag ratio. The third reason is related to the static stability condition. As the aerodynamic center behind the c.g. moves forward as the flight Mach number increases, it is hard to realize the longitudinal static stability in the hypersonic region. By the way, the PCTJ engines account for approximately half of the gross weight, as the weight breakdowns in Table 3 illustrate. The c.g. of a short and fat vehicle is near the engines, which means that it is near the rear. Therefore the short and fat vehicle has difficulty maintaining the static stability in the hypersonic region because the difference between its c.g. and its aerodynamic center is small. In the future, we must analyze body strength which is not considered in this paper.

Because each engine of the vehicle with a small number of engines is large, the aerodynamic center in the hypersonic region and the c.g. of the vehicle are near the c.g. of the engines. That means it is difficult for the vehicle with a few engines to meet the static stability requirement in the hypersonic region. Therefore the two-engine vehicle has relatively small engines for the vehicle. Though this study constrains the longitudinal static stability condition, there is an argument that, if the performance of the vehicles with the stability worsened, the condition would be unnecessary because the control system compensates for instability.

Figures 6–8 show the aerodynamic coefficients (at elevon deflection $\delta_e = 0$ [deg]) of the optimal two-engine vehicle. Figure 8

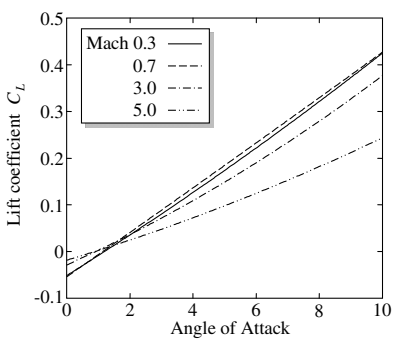

Fig. 6 Lift coefficient of two-engine vehicle.

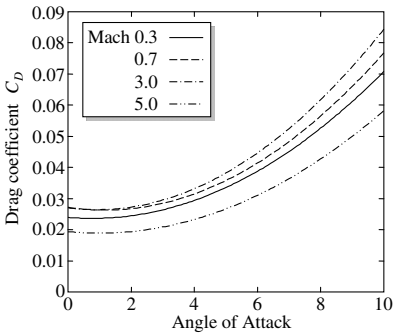

Fig. 7 Drag coefficient of two-engine vehicle.

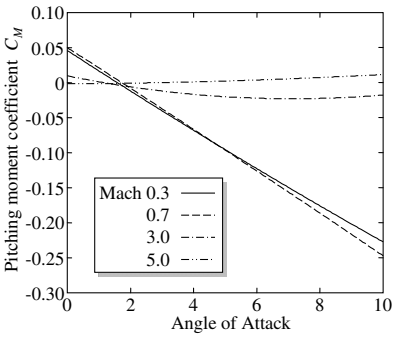

Fig. 8 Pitching moment coefficient of two-engine vehicle.

is the pitching moment coefficients about the c.g. of the vehicle (57% of the fuselage length). Though the propellant consumption moves the c.g. during the flight, the movement is less than 1% because the ratio of the propellant weight is not large. As described above, Fig. 8 suggests that it is difficult to maintain the static stability in the hypersonic region. The optimization provides the solution at the very limit of the static stability at the trim condition.

Figures 9–13 show the optimal flight trajectories. The vehicle takes off and accelerates to Mach 5 at full throttle. The takeoff speeds, which are not specified in the problem definition, are about

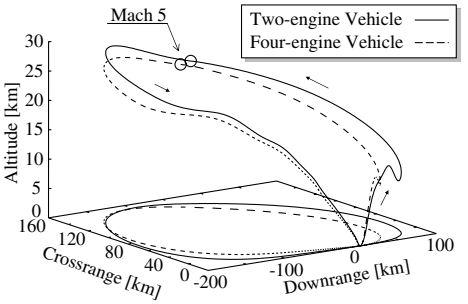

Fig. 9 Trajectory plots.

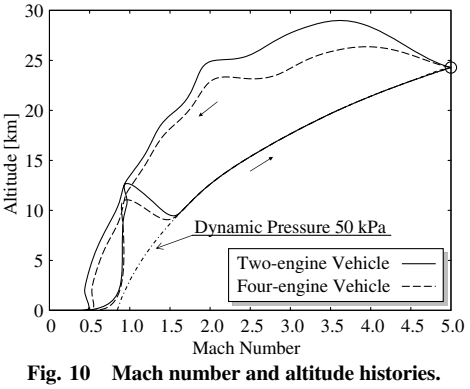

Fig. 10 Mach number and altitude histories.

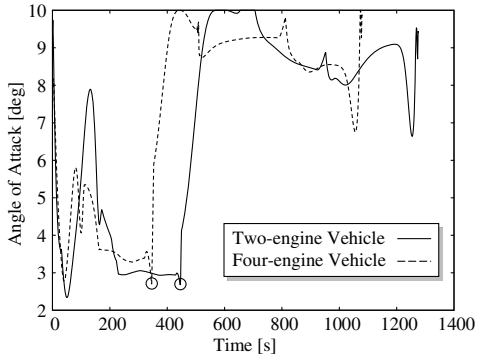

Fig. 11 Angle of attack histories.

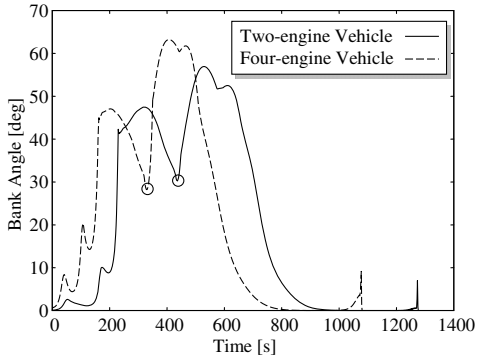

Fig. 12 Bank angle histories.

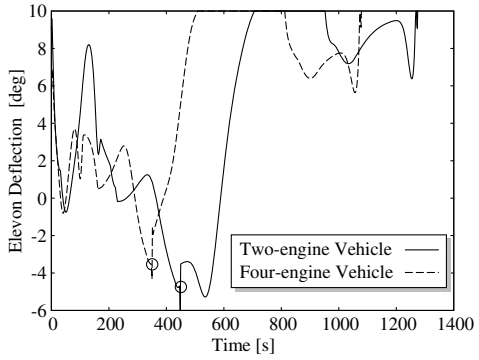

Fig. 13 Elevon deflection histories.

125 m/sec. As described above, the two-engine vehicle has proportionately smaller engines than the four-engine vehicle. As the acceleration of the two-engine vehicle is inferior, its flight time is 200 s longer than that of the four-engine vehicle and its flight range is also longer. In particular, it takes a long time for the two-engine vehicle to exceed sonic speed. With the small-scale engines, the vehicles cannot both accelerate and climb against drag divergence in the transonic range. Therefore the dynamic pressure lowered by gaining altitude at an almost constant speed reduces the drag, and then the vehicle breaks sonic speed by diving. Such a trajectory is often observed in optimal ascent trajectories of winged space transportation vehicles with airbreathing engines [1]. In general, the higher the dynamic pressure, the better the engine performance. If large engines were installed, flight along not such a trajectory but the largest dynamic pressure would be preferable. However large engines increase the gross weight of the vehicle. On the other hand, too-small engines also increase the gross weight because slow acceleration and long flight time in the transonic region increase the propellant consumption. The optimal size of the engines is thus decided based on the tradeoff relationship between them. In the supersonic and hypersonic regions, the vehicles fly along the dynamic pressure limit of 50 kPa. After reaching Mach 5, the

Table 4 Optimal configurations and component weights of case 2

Parameters	Two-engine vehicle	Four-engine vehicle
l_f, m	12.84	13.09
w_f, m	1.93	1.97
h_f, m	0.39	0.39
θ_f, deg	3.0	3.0
c_w, m	3.21	3.27
Λ, deg	51.8	55.7
A_{POTJ}, m^2	0.475	0.609
Fuselage, kg	538	590
Wing, kg	152	204
Vertical tail, kg	56	55
PCTJ, kg	2010	2926
Thrust structure, kg	68	78
Tank, kg	199	210
Thermal protection system, kg	232	233
Landing gear, kg	126	167
Subsystem, kg	442	566
Propellant, kg	596	631
Gross weight, kg	4419	5660

vehicles shut all the engines off and glide. Flight without thrust in the return phase minimizes propellant consumption and gross weights. The glide return to the takeoff point requires a turning flight in the acceleration phase. The vehicles glide at a high angle of attack, which increases the lift-to-drag ratio, and the elevon deflections are also large so as to trim the vehicle. The lift-to-drag ratio at the supersonic cruise is about 4. The flights of the two- and four-engine vehicles have the same features.

B. Case 2: Straight Flight in the Acceleration Phase

In case 2, the vehicles keep their bank angles at zero in the ascent phase. Table 4 and Figs. 14 and 15 indicate the configurations of the optimal vehicles. The characteristics of the vehicles are almost the same as those of case 1. However the vehicles cannot fly without the thrust of the engines in the return phase, because a long downrange in the ascent phase makes it impossible to return to the takeoff point by gliding alone. Therefore propellant consumption increases, and the vehicles are larger than those in case 1.

Figures 16–20 show the flight trajectories. The vehicles accelerate at full throttle. After reaching Mach 5, the engines shut off for glide flight and the vehicles begin a turn with a high bank angle. As the ground projection of the flight path points to the takeoff point, the engines ignite temporarily to increase the flight range back to the takeoff point. Because constant engine use in the turning flight increases the crossrange, the optimal solution uses temporary

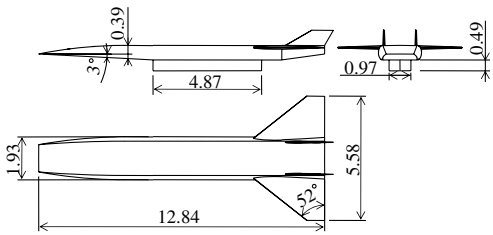

Fig. 14 Optimal two-engine vehicle.

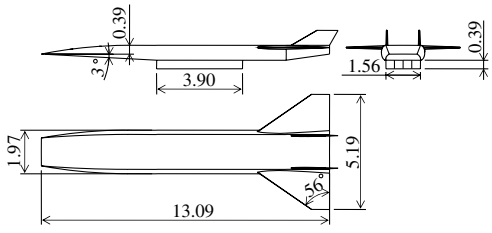

Fig. 15 Optimal four-engine vehicle.

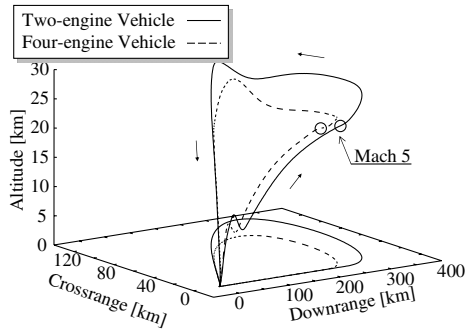

Fig. 16 Trajectory plots.

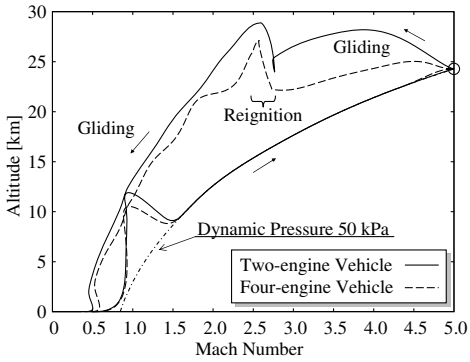

Fig. 17 Mach number and altitude histories.

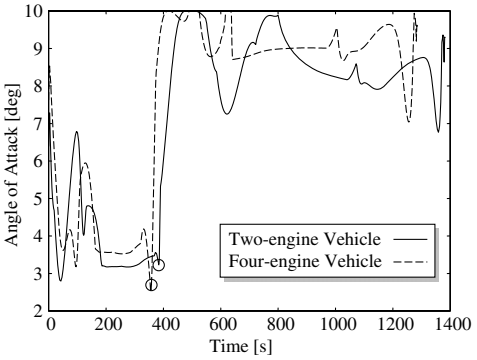

Fig. 18 Angle of attack histories.

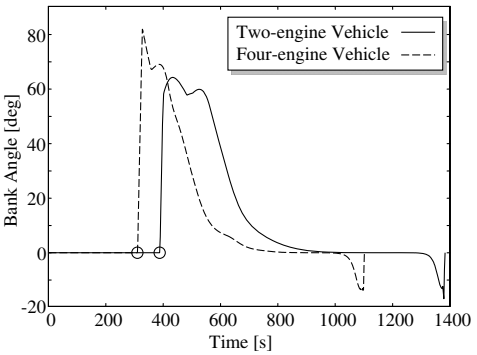

Fig. 19 Bank angle histories.

throttling to suppress the propellant consumption. It is difficult for the vehicles to approach the runway at an azimuth angle of 0 deg with large turning flights. That is why we defined the terminal condition such that the terminal azimuth angle is equal to 180 deg.

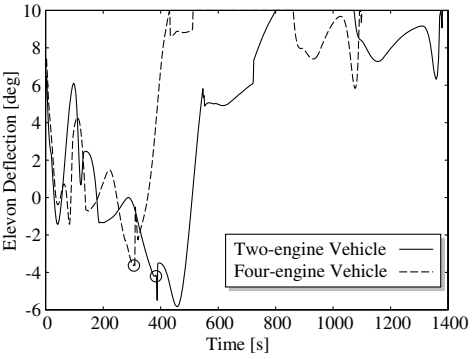

Fig. 20 Elevon deflection histories.

IV. Summary

This study aimed to configure lifting body-shaped experimental vehicles to demonstrate the performance of a hypersonic engine (precooled turbojet engine). We applied an optimization method to the conceptual designs of these vehicles to obtain the smallest vehicles that can accomplish the mission requirements. First the analysis tools were provided: the vehicle definition, the weight estimation, the aerodynamics analysis, the propulsion analysis, and the trajectory analysis. Next we integrated the analyses to specify the optimization problem. We defined the gross weight of the vehicle as a minimized parameter to find the best vehicle configurations and flight trajectories. The optimal vehicles were estimated to be about 12 m in total length and 4–5 Mg in gross weight. This study also simultaneously optimized the flight trajectories and vehicle configurations. The optimal trajectories consist of acceleration flights at full throttle and gliding return flights. The optimization demonstrates the optimal flight trajectories for minimizing the propellant consumption. Through this study, we confirmed the effectiveness of the proposed analysis and optimization method across multiple disciplines.

In the future, we must verify the optimal solutions in this study with higher fidelity methods. The recomputation of the aerodynamic forces with CFD methods and the weight analysis with structural analysis are necessary. At present, we conduct CFD analyses and wind tunnel tests for a vehicle model based on the optimal solutions. We also analyze the interference drag between the airframe and engines and the effects of the forebody compression and external nozzle which are not considered in this paper. Moreover structural analysis including structural styles of the vehicle is conducted. In the future, we will carry out numerical optimization that incorporates the results from the high fidelity analyses.

Acknowledgments

This research was partially supported by a Grant-in-Aid for Young Scientists (B), 16760642, 2005, from the Ministry of Education, Science, Sports and Culture, Japan. A data offer and analytical work were done as collaborative research with the Japan Aerospace Exploration Agency.

References

[1] Tsuchiya, T., and Mori, M., "Optimal Design of Two-Stage-to-Orbit Space Planes with Airbreathing Engines," *Journal of Spacecraft and Rockets*, Vol. 42, No. 1, 2005, pp. 90–97.

[2] Taguchi, H., Futamura, H., Yanagi, R., and Maita, M., "Analytical Study of Pre-Cooled Turbojet Engine for TSTO Spaceplane," AIAA Paper 2001-1838, 2001.

[3] Taguchi, H., Sato, T., Kobayashi, H., Kojima, T., Okai, K., Fujita, K., and Ohta, T., "Design Study on a Small Pre-Cooled Turbojet Engine for Flight Experiments," AIAA Paper 2005-3419, 2005.

[4] Harloff, G. J., and Berkowitz, B. M., "HASA: Hypersonic Aerospace Sizing Analysis for Preliminary Design of Aerospace Vehicles," NASA CR-182226, 1988.

[5] Epton, M. A., and Magnus, A. E., "PAN AIR: A Computer Program for Predicting Subsonic or Supersonic Linear Potential Flows About

Arbitrary Configurations Using a Higher Order Panel Method, Vol. 1: Theory Document (Ver. 3.0)," NASA CR-3251, 1991.
[6] Pittman, J. L., "Application of Supersonic Linear Theory and Hypersonic Impact Methods to Three Nonslender Hypersonic Airplane Concepts at Mach Numbers from 1.10 to 2.86," NASA TP-1539, 1979.
[7] Liepmann, H. W., and Roshko, A., *Elements of Gasdynamics*, Dover, New York, 2001.
[8] Palitz, M., "Measured and Calculated Flow Conditions on the Forward Fuselage of the X-15 Airplane and Model at Mach Numbers from 3.0 to 8.0," NASA TN D-3447, 1966.
[9] Maughmer, M., Ozoroski, L., Straussfogel, D., and Long, L., "Validation of Engineering Methods for Predicting Hypersonic Vehicle Control Forces and Moments," *Journal of Guidance, Control, and Dynamics*, Vol. 16, No. 4, 1993, pp. 762–769.
[10] Bonner, E., Clever, W., and Dunn, K., "Aerodynamic Preliminary Analysis System 2, Part 1: Theory," NASA CR-182076, 1991.
[11] White, F. M., *Viscous Fluid Flow*, McGraw–Hill, New York, 1991.
[12] Poggio, T., and Girosi, F., "Networks for Approximation and Learning," *Proceedings of the IEEE*, Vol. 78, No. 9, 1990, pp. 1481–1497.
[13] Yokoyama, N., Suzuki, S., Tsuchiya, T., Taguchi, H., and Kanda, T., "Multidisciplinary Design Optimization of SSTO Space Plane Considering Rigid Body Characteristics," AIAA Paper 2005-0710, 2005.
[14] Zipfel, P. H., *Modeling and Simulation of Aerospace Vehicle Dynamics*, AIAA, Reston, VA, 2000.
[15] Hargraves, C. R., and Paris, S. W., "Direct Trajectory Optimization Using Nonlinear Programming and Collocation," *Journal of Guidance, Control, and Dynamics*, Vol. 10, No. 4, 1987, pp. 338–342.

N. Alexandrov
Associate Editor